

# Optical analyses of the formation of a silver nanoparticle-containing layer in glass

Stefan Wackerow and Amin Abdolvand\*

School of Engineering, Physics & Mathematics, University of Dundee, Dundee DD1 4HN, UK  
\*a.abdolvand@dundee.ac.uk

**Abstract:** We present results of our observations on the formation of a silver nanoparticle-containing layer in glass over time. First, silver ions are driven into the glass by field-assisted ion exchange at 300 °C. A following annealing step at 550 °C resulted in the formation of silver nanoparticles (< 4 nm in diameter). This annealing was performed for *five* different durations (1h, 2h, 4h, 8h, 48h), and thin slices of the cross sections of the glasses have been prepared. The sequence of slices showed the growth of the nanoparticle-containing layer over time. Transmission spectra of the slices have been measured with a spatial resolution of 1.5 μm. Simulating spectra using the Maxwell-Garnett theory allowed us to determine the volume filling factor distribution of the nanoparticles across the layers. A first attempt to simulate the diffusion of silver is performed.

© 2012 Optical Society of America

**OCIS Codes:** (160.4236) Nanomaterials; (160.4670) Optical Materials; (160.2750) Glass and other amorphous materials.

---

## References and links

1. P. Chakraborty, "Metal nanoclusters in glasses as non-linear photonic materials," *J. Mater. Sci.* **33**(9), 2235–2249 (1998).
2. F. Gonella and P. Mazzoldi, *Handbook of Nanostructured Materials and Nanotechnology* (Academic Press 2000).
3. H. Mertens and A. Polman, "Plasmon-enhanced erbium luminescence," *Appl. Phys. Lett.* **89**(21), 211107 (2006).
4. M. Volkan, D. L. Stokes, and T. Vo-Dinh, "A new surface-enhanced Raman scattering substrate based on silver nanoparticles in sol-gel," *J. Raman Spect.* **30**(12), 1057–1065 (1999).
5. A. Stalmashonak, A. Abdolvand, and G. Seifert, "Metal-glass nanocomposite for optical storage of information," *Appl. Phys. Lett.* **99**(20), 201904 (2011).
6. U. Kreibitz and M. Vollmer, *Optical Properties of Metal Clusters* (Springer, 1995).
7. V. M. Shalaev, *Optical Properties of Nanostructured Random Media* (Springer, 2001).
8. K. L. Kelly, E. Coronado, L. L. Zhao, and G. C. Schatz, "The optical properties of metal nanoparticles: the influence of size, shape, and dielectric environment," *J. Phys. Chem. B* **107**(3), 668–677 (2003).
9. M. S. Gudiksen, L. J. Lauhon, J. Wang, D. C. Smith, and C. M. Lieber, "Growth of nanowire superlattice structures for nanoscale photonics and electronics," *Nature* **415**(6872), 617–620 (2002).
10. A. Berger, "Concentration and size depth profile of colloidal silver particles in glass surfaces produced by sodium-silver ion-exchange," *J. Non-Cryst. Solids* **151**(1-2), 88–94 (1992).
11. Y. Ma, J. Lin, S. Qin, N. Zhou, Q. Bian, H. Wei, and Z. Feng, "Preparation of Ag nanocrystals embedded silicate glass by field-assisted diffusion and its properties of optical absorption," *Solid State Sci.* **12**(8), 1413–1418 (2010).
12. S. Wackerow, G. Seifert, and A. Abdolvand, "Homogenous silver-doped nanocomposite glass," *Opt. Mater. Express* **1**(7), 1224–1231 (2011).
13. S. I. Najafi, *Introduction to Glass Integrated Optics* (Artech House, 1992).
14. S. Wackerow and G. Seifert, "Co-doping of glasses with rare earth ions and metallic nanoparticles for frequency up-conversion," *Proc. SPIE* **7725**, 77251H, 77251H-10 (2010).
15. E. Cattaruzza, G. Battaglin, F. Gonella, S. Ali, C. Sada, and A. Quaranta, "Characterization of silicate glasses doped with gold by solid-state field-assisted ion exchange," *Mater. Sci. & Eng. B: Solid-State Mater. for Adv. Tech.* **149**, 195–199 (2008).
16. D. Salazar, H. Porte, and H. Márquez, "Optical channel waveguides by copper ion-exchange in glass," *Appl. Opt.* **36**(34), 8987–8991 (1997).
17. R. S. Varma, D. C. Kothari, and R. Tewari, "Nano-composite soda lime silicate glass prepared using silver ion exchange," *J. Non-Cryst. Solids* **355**(22-23), 1246–1251 (2009).
18. R. Araujo, "Colorless glasses containing ion-exchanged silver," *Appl. Opt.* **31**(25), 5221–5224 (1992).

19. E. Borsella, E. Cattaruzza, G. De Marchi, F. Gonella, G. Mattei, P. Mazzoldi, A. Quaranta, G. Battaglin, and R. Polloni, "Synthesis of silver clusters in silica-based glasses for optoelectronics applications," *J. Non-Cryst. Solids* **245**(1-3), 122–128 (1999).
20. A. Hilger, M. Tenfelde, and U. Kreibig, "Silver nanoparticles deposited on dielectric surfaces," *Appl. Phys. B* **73**(4), 361–372 (2001).
21. B. Lamprecht, A. Leitner, and F. R. Aussenegg, "Femtosecond decay-time measurement of electron-plasma oscillation in nanolithographically designed silver particles," *Appl. Phys. B-Lasers & Opt.* **64**(2), 269–272 (1997).
22. G. Xu, M. Tazawa, P. Jin, and S. Nakao, "Surface plasmon resonance of sputtered Ag films: substrate and mass thickness dependence," *Appl. Phys., A Mater. Sci. Process.* **80**(7), 1535–1540 (2005).
23. D. Manikandan, S. Mohan, P. Magudapathy, and K. G. M. Nair, "Blue shift of plasmon resonance in Cu and Ag ion-exchanged and annealed soda-lime glass: an optical absorption study," *Physica B* **325**, 86–91 (2003).
24. S. Thomas, S. K. Nair, E. M. A. Jamal, S. H. Al-Harhi, M. R. Varma, and M. R. Anantharaman, "Size-dependent surface plasmon resonance in silver silica nanocomposites," *Nanotechnology* **19**(7), 075710 (2008).
25. K. Yata and T. Yamaguchi, "Ostwald ripening of silver in glass," *J. Mater. Sci.* **27**(1), 101–106 (1992).

## 1. Introduction

Metallic nanoparticles (NPs) exhibit unique optical properties as compared to their bulk counter parts. Embedded metallic NPs in glass have attracted much interest for a very wide spectrum of applications in photonics and optoelectronics [1–5]. They show a characteristic absorption caused by the excitation of plasmon oscillations [6, 7], and their resonance frequency depends on the size [6], shape [8] and distribution [9] of the NPs.

For generating embedded silver NPs in glass, the common approach is *via* an ion exchange process, which is followed by, or combined with thermal treatment. The ion exchange can be done in a salt melt [10], or by a field-assisted ion exchange from a solid silver film [11–13]. The advantages of the latter technique are its versatility [12, 14–16], and that it does not involve hazardous chemicals. Recently, we introduced a dry technique for doping glass with silver ions and fabrication of a homogenous silver-doped nanocomposite glass [12]. The process relied on a solid-state field-assisted diffusion process for doping silver ions into the glass matrix followed by a post-annealing step in air, leading to the formation of silver NPs. The thermal treatment at 550 °C essentially led to the reduction of the silver ions to atoms and formation of silver nanoparticles. A thin slice of the cross section of the sample was prepared that allowed visualization of its depth profile and facilitated further optical analyses of the nanocomposite. Based on our observations, we concluded that the process resulted in the formation of a nanoparticle-containing layer, where larger NPs with lower number density were formed close to the surface and smaller NPs with higher number density in the lower layers. These observations raised the question on influence of various process parameters on the thickness of the nanoparticle-containing layer and number density of the inclusions.

In this paper, we consider thin slices of *five* samples with different durations of the thermal treatment. We studied the development of the nanoparticle-containing layer over time. Utilizing the Maxwell-Garnett effective medium theory allowed us to simulate the measured absorption spectra, giving us a way to assess the volume filling factors of the NPs. The dielectric function of the NPs was calculated using the Drude Model with a particle-size-dependent dampening constant, which facilitated us to make conclusions about actual particle sizes. The temporal development of the filling factor profiles was compared with a simple diffusion model using Fick's law.

## 2. Experimental methods for preparation of the samples

Commercial Schott B270 glass with a composition of (in wt-%), (69.2) SiO<sub>2</sub>, (9.8) Na<sub>2</sub>O, (9.5) CaO, (7.6) K<sub>2</sub>O, (2.8) BaO, (1.1) Al<sub>2</sub>O<sub>3</sub> and a thickness of 1 mm, refractive index of 1.523, density of 2.55 g/cm<sup>3</sup> was used as a substrate. Following the procedure outlined in [12], a suspension of silver flakes in isopropanol was applied on one side of the glass surface. The substrate was then heated up to 300°C for 20 min. This results in the formation of an oxidized solid silver film, which later acts as a source for silver ions. The glass was then again heated up to 300°C and this time a voltage of 1 kV was applied across the sample for one hour. The silver film acted as the anode for the voltage, while a carbon foil electrode on the

opposite side of the glass acted as the cathode. At these temperatures alkali ions in the glass become mobile, and the voltage drives the residual positive ions of the glass towards the cathode. There they become neutralized, while under the anode vacancies are forming, which are filled by silver ions from the silver oxide film anode [12].

Afterwards the sample was cut into *five* pieces, and the pieces were annealed in air at 550°C, each for a different duration as follows: 1h, 2h, 4h, 8h, and 48h. This resulted in the formation of silver nanoparticles inside the glass, changing the color of the glass to dark yellow for short annealing times and brown for longer times. The glass substrate used here (B270) is known to have a very low concentration of iron, which is often considered as a reducing agent for silver during annealing process. We have recently proposed the reduction by non-bridging oxygen (NBO) [12, 17–19] and by the reaction of  $\text{Ag}^+$  to Ag and  $\text{Ag}^{2+}$  [11].

Thin slices of the cross sections allowed visualization of their depth profile. These were prepared by cutting the samples and embedding them in an epoxy resin (Specifix-20, Struers Limited) to prevent chipping of the glass and to make it physically manageable for grinding, polishing etc. The resin cures at room temperature. Each section has been polished on both sides providing slide thicknesses in the range of 30 - 33  $\mu\text{m}$ .

The optical characterizations of the sample were performed using a JASCO V-670 UV/VIS/NIR Spectrophotometer, a microscope spectrophotometer (MPM 800 D/UV, Zeiss), and KEYENCE Digital Microscope VHX-1000.

### 3. Theoretical background

Metal nanoparticles show a characteristic optical absorption band caused by surface plasmon resonances ( $\omega_{SP}$ ) [6]. The position of  $\omega_{SP}$  is determined by the dielectric functions of the host material ( $\epsilon_h$ ) and the metal nanoparticle ( $\epsilon_i$ ):

$$\text{Re} \epsilon_i(\omega_{SP}) = \epsilon_h \quad (1)$$

In this work, we are interested in the optical properties of silver nanoparticles embedded in glass mostly in the visual spectral range. The glass forming the host material is characterized sufficiently well by a constant value for  $\epsilon_h$ . The silver inclusions, on the other hand, are showing frequency-dependent refraction and absorption, which is characterized by a frequency-dependent complex dielectric function. It can be approximated using the Drude model:

$$\epsilon_i(\omega) = \epsilon_b + 1 - \frac{\omega_p^2}{\omega^2 + i\gamma\omega} \quad (2)$$

Here  $\epsilon_b$  is the bound electron dielectric function,  $\omega_p$  the electron plasma frequency and  $\gamma$  is the damping constant of electron oscillations. For a bulk metal,  $\gamma$  is the ratio of the Fermi velocity  $v_F$  and the mean free path of the electrons  $L$ . We know that our samples contain very small silver nanoparticles, as they are too small to be seen with an electron microscope with a resolution of 10 nm. Since the particle radius  $r$  is comparable to, or smaller than, the electron mean free path, scattering of electrons at the particle surface increases the dampening factor. There have been different approaches to compute the dampening effect, with all of them resulting in the term  $A v_F / r$ , with different factors  $A$ . Therefore, the dampening constant is [20]:

$$\gamma = \frac{v_F}{L} + A \frac{v_F}{r} \quad (3)$$

The size-dependent dampening results in a broadening of the plasmon band for smaller particles. Values used in this work are  $\omega_p = 9.2$  eV [21],  $\epsilon_b = 5.2$  [22],  $v_F = 1.38 \cdot 10^6$  m/s [23, 24],  $L = 57$  nm [24], and  $A = 2$  [20].

The Maxwell-Garnett theory (MGT) is used to simulate the optical properties of the analyzed samples. It is an effective medium theory, giving an effective complex dielectric function for a composite medium:

$$\varepsilon_{eff}(\omega) = \varepsilon_h \frac{(\varepsilon_i + 2\varepsilon_h) + 2f(\varepsilon_i - \varepsilon_h)}{(\varepsilon_i + 2\varepsilon_h) - f(\varepsilon_i - \varepsilon_h)} \quad (4)$$

Here,  $f$  is the volume filling factor of the nanoparticles. The MGT well describes the position and shape of the surface plasmon resonance, and its dependence on the filling factor [7]. It does not however consider multipole interactions, which are not relevant for the small particle sizes and low filling factors of the examined samples. The absorbance,  $a$ , of an effective medium can hence be calculated from its effective dielectric function:

$$a = -\ln T = l \frac{2\omega}{c} \text{Im} \sqrt{\varepsilon_{eff}(\omega)} \quad (5)$$

Here,  $c$  is the light velocity and  $l$  is the thickness of the nanocomposite. This has a great practical value since it delivers the filling factor for each measured spectrum. For example, the filling factors fitted for all the spectra measured through one nanoparticle-containing layer will show the filling factor profile of the sample. Since this has been done for samples that have been annealed for different durations, the resulting profiles show the growth of the nanoparticle-containing layer over time. Figure 1 demonstrates an example of one such analysis.

This growth is the result of the diffusion of silver, either in ionic or atomic form. It is a rather complex process, which is approximated in this work with the rather simple Fick's law:

$$\frac{\partial f}{\partial t} = D \frac{\partial^2 f}{\partial x^2} \quad (6)$$

Here,  $D$  is the diffusion coefficient of silver. It describes the development of the silver filling factor profile over time. This formula is neglecting any change in concentration of the diffusing silver by the agglomeration in nanoparticles or differences in the behavior of atomic and ionic silver.

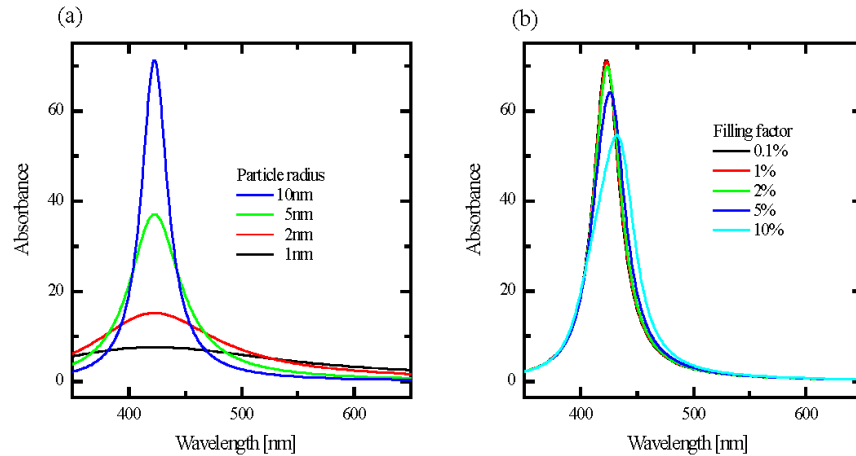


Fig. 1. (a) Particle size dependence for  $f = 0.1\%$  and a layer thickness of  $100 \mu\text{m}$ . (b) Filling factor dependence for particle radius of  $10 \text{ nm}$ , and a layer thickness proportional to  $1/f$  (in order to make the plasmon bands comparable).

## 4. Results and discussion

### 4.1 Spectral profiles of the cross sections

Figure 2(a) shows microscope images of the thin slices. These are the cross sections of the generated silver nanoparticle-containing layers. Figure 2(b) presents the absorbance profiles measured on these thin slices. These graphs show how the plasmon band changes in the depth of the glass with longer annealing times. For 1h annealing the plasmon band at the surface is centered at about 430 nm. In the lower layers the plasmon band becomes much wider, similar to the simulated plasmon bands for very small nanoparticles. In the deeper layers of the glass the absorbance decreases. Both effects are caused by a low amount of silver located in nanoparticles in these regions. It has to be pointed out that the maximum absorbance could only be measured correctly for the deepest layers with lower particle concentrations (since it was too high for most of the glass due to the very high volume filling factor of the NPs in these regions). Therefore the exact plasmon band position and height could not be determined, however what has been measured allowed us to make the following conclusions.

For longer annealing times the silver spreads out into deeper layers. The nanoparticle-containing layer becomes thicker. Near the surface the plasmon band becomes narrower, which fits to the simulated spectra for growing particle sizes. This can either happen by the agglomeration of more silver or by Ostwald ripening [25]. In this process smaller NPs are dissolved and redeposited onto larger NPs. At the depths where the shorter-annealed samples have a wide plasmon band, the width decreases strongly and the plasmon bandwidth at the lowest edge of the profile is slightly lower for longer annealing times. This means that NPs already have a larger size when they reach a comparable concentration. Since the rate at which the thickness of the layers grows is decreasing one could conclude that the growth of the particle sizes does not slow down as much with longer annealing times as with the increase of the layer thickness.

### 4.2 Fitting of the spectra

The MGT is used to make a fit to the plasmon bands of the measured spectra. Fitting parameters have been the filling factors and particle radii. Another model parameter is the thickness of the particle-containing layer  $l$ , which is the thickness of the slice in this case. This has been computed by summing up all the absorbance spectra  $a_i$  measured on one thin slice, and fitting that to the absorbance spectrum  $a_{tot}$  measured through the sample before cutting the slice, in accordance with:

$$a_{tot} = \frac{1.5\mu m}{l} \sum a_i + a_0 \quad (7)$$

The value  $a_0$  has to be added to account for the surface reflections. This provided theoretical slice thicknesses of 28.7  $\mu\text{m}$ , 34.0  $\mu\text{m}$ , 31.1  $\mu\text{m}$ , 23.4  $\mu\text{m}$  and 21.9  $\mu\text{m}$ , for the 1h, 2h, 4h, 8h and 48h annealed slices, respectively. These values are very close to the experimentally determined value for the thickness of the polished thin slides of  $\sim 30 \mu\text{m}$  (please see the Experimental Methods).

The obtained fitting parameters are shown in Fig. 3 as solid lines. The filling factors are plotted in the left graph and the particle radii in the right graph, both as a function of the position where the spectra were measured. For large parts of the thin slices we were unable to find reliable values since the peaks of the plasmon bands were not measured. These values have been removed from the graphs, therefore only the values from the deepest particle-containing layers with lower concentration are plotted. The obtained filling factor values at the glass surface have been plotted to show the actual surface position and the maximum measurable slopes.

The shown filling factor profiles are similar to diffusion profiles, comparable to the ones obtained for silver ions diffusing in glass [13]. They show a gradual decrease of the filling factor with the depth, and the slope becomes more flat for longer annealing times, as it should

be for diffusion. The thickness of the nanoparticle-containing layers  $T_L$  of the whole uncut sample has been determined from the filling factor profiles. At a value of  $f = 0.05\%$  the following thicknesses have been obtained:  $76\mu\text{m}$  after 1h,  $97\mu\text{m}$  after 2h,  $115\mu\text{m}$  after 4h,  $135\mu\text{m}$  after 8h and  $214\mu\text{m}$  after 48h. These values are very close to the experimentally measured thicknesses, as can be seen in Fig. 2(a). These values roughly follow a logarithmic growth, to which a function has been fitted:

$$T_L = 70.8\mu\text{m} + 35.5\mu\text{m} \ln t \quad (8)$$

where  $t$  is the annealing time in hours. The particle radii graphs show the behavior described earlier. The particle size is decreasing at the low filling factor end, and the particles become larger for longer diffusion times.

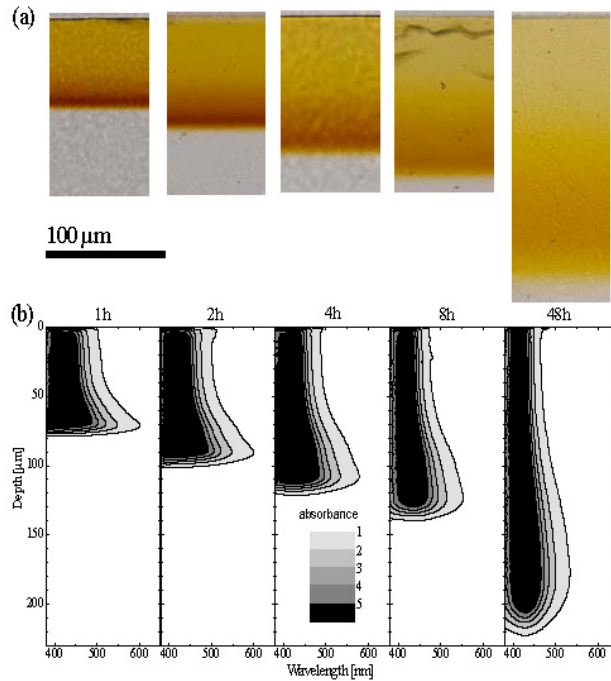


Fig. 2. Thin slices of the cross sections have been prepared from samples annealed for *five* different durations (1h, 2h, 4h, 8h, 48h). (a) Microscope images of the thin slices. The former glass surfaces are at the top of the image, while the lower parts of the image show the layers deeper inside the glass. For short annealing times the nanoparticles cause a dark yellow color close to the surface, which changes to brown at the inner end of the layer. For longer annealing times the color at the surface changes to light yellow, while it turns to a darker yellow for the inner regions. (b) Absorbance spectra of the *five* slices. The depth in the glass is assigned to the vertical axis, while the wavelength is assigned to the horizontal axes. The former glass surface is at the bottom end. Darker colors stand for stronger absorbance. One spectrum has been measured every  $1.5\mu\text{m}$ .

#### 4.3 Diffusion simulation

A diffusion simulation has been done to determine the higher filling factor parts of the profiles and the diffusion coefficient. A simple diffusion process has been assumed, described by Fick's law. The starting profile of the diffusion is the silver concentration profile of the glass directly after ion exchange. A backscattering electron microscopy image of the ion-exchanged glass (before cutting and annealing the sample for different durations) showed a well-confined homogeneous silver layer of  $21.5\mu\text{m}$  just below the surface. The concentration of silver in this layer has been determined by EDX to be approximately 15 atom-%. This has to be converted to the volume concentration in order to simulate the filling factor. From the

known composition of the B270 glass we calculated its molar density to be  $0.041 \text{ mol/cm}^3$ . This means that the silver concentration was  $0.0061 \text{ mol/cm}^3$ . The nanoparticles are assumed to have a density comparable to macromolecular silver, which has a molar density of  $0.0972 \text{ mol/cm}^3$ . From the latter two values results in a volume filling factor of  $\sim 6.3\%$ .

The numerical simulation was done by doing a one-dimensional approximation of Fick's law using the Finite difference method [14]. The whole thickness of the glass of  $1 \text{ mm}$  was simulated, with a resolution of  $0.15 \text{ }\mu\text{m}$ . The time step size was  $0.02 \text{ s}$ , and the simulation was initialized with a step profile with  $6.3\% \text{ Ag}$  in the first  $21.5 \text{ }\mu\text{m}$ .

The diffusion coefficient  $D$  has been fitted by minimizing the sum of the squares of the difference between the filling factor profile after  $1 \text{ h}$  and the simulated diffusion profile after  $1 \text{ h}$ . The obtained value for diffusion coefficient of silver at  $550 \text{ }^\circ\text{C}$  was then obtained to be  $D = 0.098 \text{ }\mu\text{m}^2 / \text{s}$ . With this value the diffusion was also simulated for longer durations. The resulting profiles and the filling factor profiles are shown in Fig. 3(a) – the filling factor profiles are shown as solid lines and the diffusion simulation results as dotted lines.

The position in the depth of the glass matches quite well for the profiles simulated for  $1, 2$  and  $4 \text{ h}$  diffusion times. However for longer annealing times the simulation shows a distinctly deeper diffusion than the particle filling factor profiles. Also the trend is different, since the distance of the particle filling factor profiles becomes smaller for a doubling of the diffusion time, while the diffusion simulation results in increasing distances.

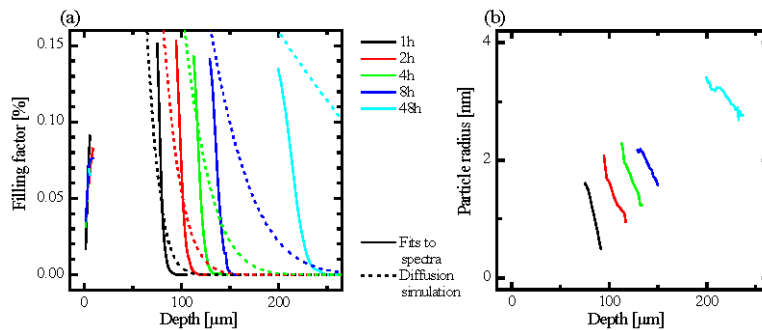


Fig. 3. Fitting parameters for the plasmon band profiles measured on the thin slices (solid lines). The filling factor profiles are shown in (a) and the particle radii in (b), both as a function of the depth in the glass. Only the low-concentration end is shown since the concentration was too high in most of the sample to determine it reliably. Dotted lines in (a) are the results of the diffusion simulation, with the profile for  $1 \text{ h}$  diffusion being fit to the MGT profile for the  $1 \text{ h}$  annealed sample.

For the filling factor profiles the slope measured at the glass surface ( $depth = 0$ ) is also shown in Fig. 3(a). The ideal result would be a vertical line; however the slope is  $0.02\% / \mu\text{m}$ . This results from the stray light going through the microscope beside the sample. Since these effects are comparable all over the thin slice,  $0.02\% / \mu\text{m}$  represents the maximum slope that can be measured. This slope is only reached for the  $1 \text{ h}$  profile for  $x \leq 78 \text{ }\mu\text{m}$ , where the filling factor is  $\sim 0.06\%$ . The simulated profile for  $1 \text{ h}$  annealing is less steep than the measured profile for that of diffusion time. A steeper profile can be simulated assuming a much larger initial filling factor – in fact the best fit is achieved for an impossibly high filling factor of  $4000\%$ .

The increased steepness of the actual profile and the slowing down of the actual diffusion compared to the simulated one might be the result of the gradual agglomeration of silver, hence reducing the amount of silver that is taking part in diffusion. A simulation was done assuming that the rate of decrease of the concentration is simply proportional to the concentration of the diffusing silver. This resulted in profiles similar to those obtained with a lower initial concentration. A more sophisticated approach would be necessary to describe these profiles, with a stronger effect in the low concentration area at the edge of the silver-containing layer.

## 5. Conclusion

The analyzed thin slices allowed characterization of the particle concentration profiles and particle sizes for different annealing times. From the first filling factor profile and the initial concentration profile the diffusion coefficient of silver at 550°C was determined to be 0.098  $\mu\text{m}^2/\text{s}$ . However the apparent differences between the simulated diffusion profiles and the obtained filling factor profiles show that there are other processes involved than a simple diffusion according to Fick's law. One relevant process might be the decrease of the amount of diffusing silver due to the agglomeration in nanoparticles. This would mean that the actual diffusion coefficient of silver is higher than the one determined.

This work provides valuable insight into the three-step solid-state field-assisted diffusion technique for fabrication of homogenous silver-doped nanocomposite glass [12]. Studying different annealing parameters allow one to assess their effect on the diffusion parameters, depth profile, number density and size of the inclusions. These are all of paramount importance since optical and structural properties of nanocomposites are directly influenced by the spatial distribution of inclusions.

## Acknowledgments

The authors would like to thank Dr. Gerhard Seifert of the Martin-Luther University Halle-Wittenberg/Germany for providing access to the microscope spectrophotometer (MPM 800 D/UV, Zeiss). This work was conducted under the aegis of the Engineering and Physical Sciences Research Council (EPSRC) of the United Kingdom (EP/I004173/1). Amin Abdolvand is an EPSRC Career Acceleration Fellow at the University of Dundee.